JOURNAL OF AIRCRAFT
Vol. 35, No. 5, September–October 1998

Numerical Representation of Pitching and Nonpitching Airfoils Undergoing Linear Acceleration

Jed E. Marquart*
Ohio Northern University, Ada, Ohio 45810
and
Franklin E. Eastep†
University of Dayton, Dayton, Ohio 45469

A numerical approach is presented for computing unsteady aerodynamic effects on an airfoil that is undergoing independent pitching and/or plunging motion while attached to an accelerating body. The acceleration of the body may be at any angle to the horizontal axis. Grid speed terms are incorporated into a first-order finite volume representation of the unsteady Euler equations, along with the appropriate acceleration terms for the boundary conditions. Unstructured grid methodology is utilized, along with a moving grid algorithm, to model the pitching/plunging of the airfoil within the grid. A NACA 0012 airfoil is considered for all work. Comparisons are made with nonaccelerating numerical and wind-tunnel data to demonstrate the validity of the methodology. Results are then presented for pitching and nonpitching airfoil, accelerated body cases to demonstrate the effects of the linear acceleration on the unsteady aerodynamics of the airfoil. The quantitative effect of the body acceleration on the aerodynamic coefficients is seen to be a function of the type of motion (pitching/nonpitching) imposed upon the airfoil.

Nomenclature

A = cell area
$\boldsymbol{a}$ = acceleration vector
b = airfoil semichord
C_d = section drag coefficient
C_l = section lift coefficient
c = boundary distance, airfoil chord length
e = total energy, defined in proper units for the context
$\boldsymbol{F}$, $\boldsymbol{G}$ = Euler flux vectors in x and y Cartesian directions, respectively
k = spring stiffness
$k_1(s)$ = Wagner function
L = airfoil section lift force
M_∞ = freestream Mach number
$\boldsymbol{n}$ = surface normal vector
p = fluid static pressure
$\boldsymbol{Q}$ = vector of conserved variables
s = nondimensional distance traveled
t = real time
U, V = contravariant velocities
u, v, w = Cartesian velocity components
$\boldsymbol{V}$ = velocity vector
v, w = longitudinal and vertical airfoil velocities in Wagner theory
x, y = spatial locations
x_t, y_t = grid speeds
x_{t_b}, y_{t_b} = body velocities
$x_{t_{cs}}$, $y_{t_{cs}}$ = control surface velocities
α = airfoil geometric angle of attack
γ = ratio of specific heats
Δt = real time step
δ = grid point displacement
ρ = fluid density

Presented as Paper 97-0616 at the AIAA 35th Aerospace Sciences Meeting, Reno, NV, Jan. 6–9, 1997; received July 23, 1997; revision received June 12, 1998; accepted for publication June 16, 1998.

*Associate Professor, Department of Mechanical Engineering. Senior Member AIAA.

†Professor, Department of Mechanical and Aerospace Engineering. Associate Fellow AIAA.

Introduction

EXPERIMENTAL and computational work in aeronautics has focused on the need for increased flight vehicle maneuverability, speed, endurance, and aerodynamic capabilities. These requirements arise in all types of flight vehicles, whether a military aircraft engaging another aircraft in air-to-air combat, a surface-to-air missile engaging and destroying a target, or even a commercial aircraft delivering passengers or cargo to their destination safely and efficiently. As technology progresses, and quicker responses are required, the need for faster and more efficient air vehicles becomes increasingly important.

Along with the demand for increased performance and maneuverability of flight vehicles, however, come additional challenges to the engineers and designers of the systems. Such considerations as weight, material properties, structural response to increased aerodynamic loading, economic factors, and highly complex aerodynamic interactions must be dealt with in a conscientious manner. Physical phenomena that may have been considered negligible in the past have now become important factors in the design and analysis of the system. In particular for this work, the effects of high acceleration rates on the aerodynamics experienced by the vehicle should be investigated.

The field of computational fluid dynamics (CFD) has played an increasingly vital role in the design and development process of flight vehicles, as well as many other applications. CFD techniques have been used to model airflow about complete aircraft at steady state,[1,2] analyze store (armament) separation problems,[3,4] and investigate the aeroelastic response of an aircraft structure to aerodynamic loading.[5–7] In addition, numerical techniques have been applied to investigate more basic flow physics, such as the effects of pitching and pitch rate of an airfoil on vortex generation, dynamic stall, and initial flow development.[8–10]

One area that has received very little attention is that of the unsteady aerodynamic effects on a wing or control surface because of acceleration of the body to which it is attached. In

the past, these effects have been considered minimal, and are generally neglected in favor of steady-state or quasisteady simulations because the acceleration rates achievable on the body were considered to be low. However, with improved performance of flight vehicles, the achievable longitudinal and lateral acceleration rates have increased tremendously,[11] to the point that the effects of such accelerations should be considered in the design and analysis of flight vehicles.[12] These effects may become pronounced in such analyses as dynamic stall and flutter prediction on an accelerating vehicle. For example, the effect of longitudinal acceleration on the lift coefficient for an aircraft accelerating at 0.5 g may be negligible, whereas for a missile accelerating at 12 g, the effect may be pronounced.

Very little work has been performed in the area of experimental or numerical simulation of the unsteady aerodynamic effects of a body undergoing longitudinal or transverse accelerations. Sawyer and Sullivan[13,14] experimentally investigated the unsteady lift development on a wing undergoing a change in forward speed, whereas while Ando and Ichikawa[15] developed a more classical numerical approach to analyzing an accelerating body. A general approach to modeling the aerodynamic effects on an accelerating body using CFD techniques, however, has not been developed prior to this work.

This paper describes a method of analyzing the unsteady aerodynamic effects of an airfoil attached to a body that is undergoing acceleration. The airfoil may be pitching or plunging relative to the body, or may be stationary relative to the body to which it is attached. The acceleration of the body relative to the inertial reference frame is specified by the user, in any coordinate direction. A finite volume flow solver was modified to include a moving grid algorithm for airfoil motion, as well as to include the proper acceleration terms for the airfoil motion and body acceleration.[16] The resultant code is used to determine the effects of body acceleration on the aerodynamics of a NACA 0012 airfoil, in both pitching and nonpitching modes. Various magnitudes and directions of body acceleration are investigated, and trends are established. These techniques may be used to analyze the effects of body acceleration on the aerodynamic coefficients of a wing or control surface on the body.

Governing Equations

The governing equations for the flow are the two-dimensional, unsteady Euler equations. The variables p, ρ, u, v, and e represent the pressure, density, Cartesian velocity components, and total energy, respectively.

For a control volume Ω with boundary $\partial\Omega$ moving with constant velocity in a two-dimensional Cartesian coordinate system, the equations of fluid motion may be written in integral form as

$$\frac{\partial}{\partial t}\int_{\Omega} \boldsymbol{Q}\,\mathrm{d}x\,\mathrm{d}y + \int_{\partial\Omega} (\boldsymbol{F}\,\mathrm{d}y + \boldsymbol{G}\,\mathrm{d}x) = 0 \tag{1}$$

where $\boldsymbol{Q}$ is the vector of conserved flow variables

$$\boldsymbol{Q} = \begin{Bmatrix} \rho \\ \rho u \\ \rho v \\ e \end{Bmatrix}$$

and $\boldsymbol{F}$ and $\boldsymbol{G}$ are the Euler flux vectors

$$\boldsymbol{F} = \begin{Bmatrix} \rho U \\ \rho U u + p \\ \rho U v \\ (e + p)U + x_t p \end{Bmatrix}, \qquad \boldsymbol{G} = \begin{Bmatrix} \rho V \\ \rho V u \\ \rho V v + p \\ (e + p)V + y_t p \end{Bmatrix}$$

where U and V are the contravariant velocities for the moving system, defined as $U = u - x_t$ and $V = v - y_t$. In these terms, x_t and y_t represent the grid velocities in the x and y Cartesian coordinate directions, respectively.

For the present case of an accelerating body, the grid velocities are composed of two terms; the velocity resulting from the movement of the airfoil (pitching/plunging) relative to the body ($x_{t_{cs}}$, $y_{t_{cs}}$), and the velocity of the body relative to the inertial frame of reference (x_{t_b}, y_{t_b}). Thus, the grid velocities may be given as

$$x_t = x_{t_{cs}} + x_{t_b}, \qquad y_t = y_{t_{cs}} + y_{t_b}$$

Applying this definition of the contravariant velocities to the governing Eq. (1) results in the following forms of the conserved variable and flux vectors:

$$\boldsymbol{Q} = \begin{Bmatrix} \rho \\ \rho u \\ \rho v \\ e \end{Bmatrix}, \qquad \boldsymbol{F} = \begin{Bmatrix} \rho U \\ \rho U u + p \\ \rho U v \\ (e + p)U + (x_{t_{cs}} + x_{t_b})p \end{Bmatrix}$$

$$\boldsymbol{G} = \begin{Bmatrix} \rho V \\ \rho V u \\ \rho V v + p \\ (e + p)V + (y_{t_{cs}} + y_{t_b})p \end{Bmatrix}$$

Finally, for an ideal gas, the equation of state to complete the equation set may be written as

$$p = (\gamma - 1)\rho[e - \tfrac{1}{2}(u^2 + v^2)]$$

The set of vector equations listed in the preceding text, along with the constitutive equation, were solved on an unstructured grid, upon incorporation of the proper boundary conditions, as developed for an accelerating coordinate system. The boundary conditions and flow solver used are described in the following sections.

Boundary Conditions

A major contribution of this work is that of modeling the effects of body acceleration on the aerodynamics of an airfoil that is moving or stationary relative to the body. To accomplish this task the boundary conditions must be modified to include the acceleration terms.

At the surface of the airfoil, flow tangency conditions must be imposed on the solid surface

$$\boldsymbol{V}\cdot\boldsymbol{n} = 0 \tag{2}$$

This is accomplished by setting the convective mass, momentum, and energy fluxes across the face edges that lie on the solid surface equal to zero.

The result of the flow tangency condition is that the only dependent flow variable that needs to be evaluated at the impermeable boundary for the Euler equations is pressure. To determine the expression for the pressure gradient normal to the surface at the impermeable wall, the inner product of the surface unit normal and the unsteady Euler momentum equation must be obtained. This inner product, upon simplification, takes on the following form:

$$\frac{\partial p}{\partial n} = \rho\boldsymbol{V}\cdot\frac{\partial \boldsymbol{n}}{\partial s} - \boldsymbol{n}\cdot\rho\frac{\partial \boldsymbol{V}_s}{\partial t} \tag{3}$$

where the term $\rho\boldsymbol{V}\cdot(\partial\boldsymbol{n}/\partial s)$ would be present for an impermeable wall that is stationary or moving at constant velocity, and the term $\rho(\partial\boldsymbol{V}_s/\partial t)$ represents the additional pressure gradient contribution caused by the acceleration of the solid surface.

This solid surface acceleration contribution term includes the factor $\partial\boldsymbol{V}_s/\partial t$, which represents the acceleration of the solid

surface relative to the inertial frame of reference. As such, this factor may be given as

$$\frac{\partial \boldsymbol{V}_s}{\partial t} = \boldsymbol{a}_{\text{cs}} + \boldsymbol{a}_b \tag{4}$$

where $\boldsymbol{a}_{\text{cs}}$ represents the acceleration of the control surface relative to the moving body reference frame, and $\boldsymbol{a}_b$ represents the acceleration of the body relative to the inertial frame of reference.

The acceleration of the airfoil relative to the moving body reference frame is a result of pitching or plunging of the airfoil. As the airfoil pitches or plunges, and the grid adapts to the moving airfoil, new spatial location data for each control volume edge are obtained at every time step. The velocity of each control surface is obtained using a first-order backward difference of the spatial location. Then, the acceleration is determined using a first-order backward difference in time discretization of the control surface velocities. Thus, as the airfoil pitches or plunges, the acceleration of the control surface relative to the moving body reference frame is calculated as

$$\boldsymbol{a}^n_{\text{cs}} = \frac{\boldsymbol{V}^n_{\text{cs}} - \boldsymbol{V}^{n-1}_{\text{cs}}}{\Delta t} \tag{5}$$

The acceleration of the moving body relative to the inertial frame of reference is specified by the user, and may be prescribed to vary during the run.

On the outer surface of the grid, nonreflecting fixed far-field boundary conditions are applied as described in the flow solver reference manual.[16]

Finite Volume Flow Solver

The basic flow solver used for this work is entitled Cobalt.[16] It is a finite volume flow solver that uses unstructured grid methodology and an explicit discretization formulation. Cobalt is based upon the approximate Riemann solver attributed to Colella.[17] It provides the capability of solving either the Euler or Navier–Stokes equations, along with associated turbulence models for viscous solutions. The Euler equations were solved for this work.

Cobalt is capable of handling two- or three-dimensional problems, as well as axisymmetric ones, with first- or second-order spatial accuracy, and first-, second- or third-order temporal accuracy. The problems solved during this work were two dimensional, and first-order accuracy in time and space was used.

The basic flow solver was highly modified to provide the capability of modeling an accelerating body, as well as for the inclusion of the dynamic grid algorithm for airfoil pitching and plunging motion specification. Appropriate boundary conditions were incorporated, as described previously.

Moving Grid Algorithm

As the airfoil is permitted to pitch or plunge relative to the body to which it is attached, the grid points representing the airfoil move within the grid. The surrounding grid points must, then, adapt themselves around this new airfoil position. To accomplish this task, a moving grid algorithm was incorporated, based upon the work by Batina,[18] but modified as described in the following text.

Each edge of the grid cells is modeled as a spring, as illustrated in Fig. 1. The stiffness of each of these springs is then taken to be inversely proportional to the length of the edge, as given by

$$k_m = \frac{1}{[(x_j - x_i)^2 + (y_j - y_i)^2]^{1/2}} \tag{6}$$

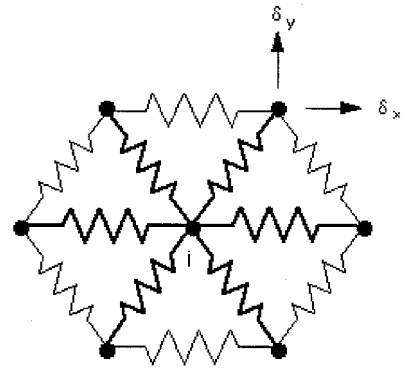

Fig. 1 Grid cell edges as springs.

where i and j are the indices of the grid points forming the endpoints of the edge.

As the airfoil moves, the grid points representing the airfoil take on the instantaneous positions of the solid surface, while the grid points representing the outer boundary (the far field) are held stationary. Using the spring analogy, a system of simultaneous equations representing the static equilibrium equations is solved iteratively at each point in time. A predictor–corrector procedure is utilized in which the predicted displacement is given by

$$\tilde{\delta}_{x_i} = 2\delta^n_{x_i} - \delta^{n-1}_{x_i}, \qquad \tilde{\delta}_{y_i} = 2\delta^n_{y_i} - \delta^{n-1}_{y_i} \tag{7}$$

where n is the current time level, and $n - 1$ is the previous time level.

The corrected displacement term is then obtained using the sum of products in the following manner:

$$\delta^{n+1}_{x_i} = \frac{\sum k_m \tilde{\delta}_{x_m}}{\sum k_m}, \qquad \delta^{n+1}_{y_i} = \frac{\sum k_m \tilde{\delta}_{y_m}}{\sum k_m} \tag{8}$$

Iteration continues using the predictor–corrector scheme until the displacement is sufficiently converged, according to a specified convergence criterion. Then, the new locations of the grid points are obtained by using the converged displacement and the previous grid locations:

$$x^{n+1}_i = x^n_i + \delta^{n+1}_{x_i}, \qquad y^{n+1}_i = y^n_i + \delta^{n+1}_{y_i} \tag{9}$$

A modification to the method for the current work was performed such that, rather than using old data for all grid points during each predictor–corrector iteration, the most current iteration is used for points that have already been examined. In this way, a Gauss–Seidel formulation is utilized, rather than the Jacobi iteration scheme used in the reference work.

For this Gauss–Seidel iteration, then, the predictor takes on the following form for the interior grid points:

$$\tilde{\delta}_{x_i} = \delta^{n+1}_{x_i}, \qquad \tilde{\delta}_{y_i} = \delta^{n+1}_{y_i} \tag{10}$$

and the form for the outer boundary and airfoil grid points becomes

$$\tilde{\delta}_{x_i} = \delta^n_{x_i}, \qquad \tilde{\delta}_{y_i} = \delta^n_{y_i} \tag{11}$$

The Gauss–Seidel iteration scheme significantly reduces the number of iterations required for convergence over the Jacobi iteration scheme. Typically, only two to three Gauss–Seidel iterations were required for convergence after a movement of the airfoil within the grid.

The unstructured grid used for computations throughout this work is illustrated in Fig. 2. It is composed of a NACA 0012

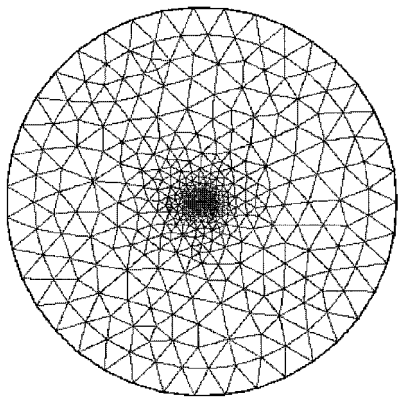

Fig. 2 Computational grid with airfoil.

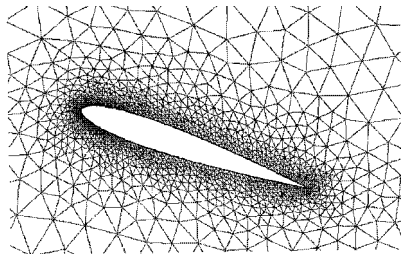

Fig. 3 Closeup of airfoil pitched plus 20 deg.

airfoil of unit chord length, with a circular outer boundary of radius 20 units, centered about the leading edge of the airfoil.

The capability of the moving grid algorithm to smoothly adapt the interior grid about the airfoil as it pitches is demonstrated in Fig. 3. Similar results were obtained for a plunging and pitching/plunging airfoil, thus demonstrating the ability of the technique to adapt the grid about a moving solid surface.

Geometric Conservation Law

To avoid the introduction of errors into the flow solution for the moving grid, a geometric conservation law must be satisfied. This conservation law is in addition to the laws that govern the physics of the flow; those of conservation of mass, momentum, and energy. Basically, the conservation law states that the rate of change of volume of the control volume must be balanced by the growth of the volume boundary.

This conservation law is given in integral form by Thomas and Lombard[19] as

$$\frac{\partial}{\partial t}\int_{\Omega} \mathrm{d}x\ \mathrm{d}y - \int_{\partial\Omega} (x_t\ \mathrm{d}y - y_t\ \mathrm{d}x) = 0 \qquad (12)$$

To solve for the current cell volume (area in two dimensions), this conservation integral may be discretized in the following manner:

$$A_i^{n+1} = A_i^n + \Delta t \sum (x_{t_m}^{n+1}\Delta y_m - y_{t_m}^{n+1}\Delta x_m) \qquad (13)$$

where the summation of the products of grid speeds and edge lengths is performed over all edges composing cell i.

As an improvement over the method of geometric conservation shown in the preceding text, this work recalculates the cell volumes, cell edge lengths, and all necessary geometric information after every iteration and grid adaption. In this way, geometric conservation is precisely ensured for all time.

Exact calculation of cell volumes and cell edge lengths provides the values necessary to utilize a backward-difference representation for the volume time derivative and the grid speeds.

Results and Discussion

Results were computed for several cases, including both pitching and nonpitching airfoils. The cases chosen were ones for which solutions have been established, and either computational or experimental results provided.

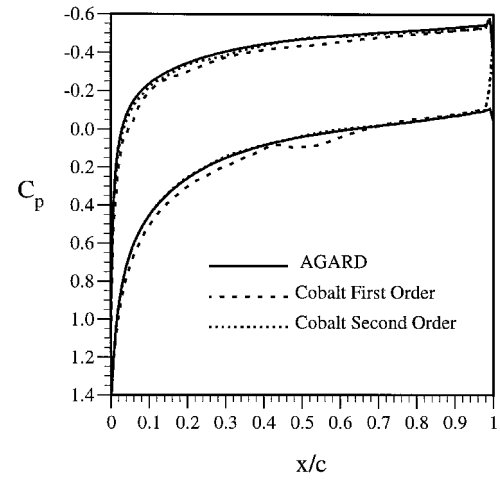

Fig. 4 C_p values for steady-state case.

For the nonpitching cases, the test cases were selected from a set of numerically derived Euler AGARD data.[20] Results were obtained for a steady-state NACA 0012 airfoil configuration to validate the basic flow solver. The correlation of pressure coefficients on the airfoil surface for the case in which $M_\infty = 1.2$ and $\alpha = 7.0$ deg is demonstrated in Fig. 4.

Both first- and second-order Cobalt results were determined to compare well with the published data. Second-order results provided the best fit with published data, but required approximately four times the computational time required for the first-order solver. For the cases examined, the second-order Cobalt solution provided a coefficient of lift value that was within 2.2% of the AGARD data value. Also, the coefficient of lift from the first-order Cobalt solution was within 0.8% of the second-order Cobalt solution value. Although this will not be true for all cases, it was determined that because it was true for the cases examined in this work, the first-order solver provided results that were close enough to the second-order results to be usable, and provided a tremendous decrease in computational time required. Therefore, the first-order algorithm was selected for use in this initial work, the flow solver was modified, and further testing was performed.

To verify the correctness of the grid speed terms, the airfoil was assigned a constant Mach number of $M_\infty = 0.9$ into the freestream, whereas the freestream Mach number was uniform at a reduced value of $M_\infty = 0.3$. This set of values provided a relative Mach number of 1.2, which is equivalent to the case described previously. A numerical solution was then obtained, and compared to the steady-state (stationary airfoil) case.

The close correlation of the moving airfoil and stationary airfoil cases is illustrated in Fig. 5. Note that the calculated surface pressure coefficients are identical for both cases, and the curves are coincident and indistinguishable. The data for both cases was obtained using the first-order flow solver.

Various combinations of airfoil Mach numbers, freestream Mach numbers, and angles of attack were modeled. The results were identical, as seen in the case just described. Thus, the representation of the grid speeds in the Euler equations was verified. The same AGARD test cases were later used for accelerated test runs.

For the pitching airfoil case, a set of wind-tunnel data for a pitching NACA 0012 was selected.[21] This case was run at $M_\infty = 0.3$, and the airfoil pitched from $\alpha = -0.03$ deg to $\alpha = 15.54$ deg over a time period of 0.01642 s. The reported approximate pitch rate was 1280 deg/s, and the Reynolds number was 2.7×10^6. Although this test case was experimental and, thus, viscosity effects were included, it was chosen because of the ramp motion of the airfoil, the short-time duration, and the complete data set availability.

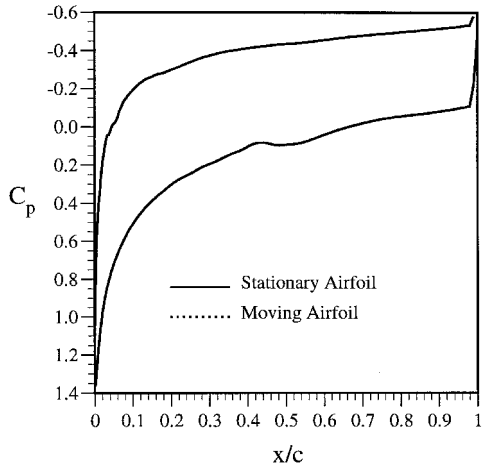

Fig. 5 C_p values for moving airfoil case.

A numerical solution was obtained for the pitching airfoil, and pressure and lift coefficients were compared to the experimental data. The close correlation of the pressure coefficients at $t = 0.0$ and 0.01642 s, respectively, is shown in Figs. 6 and 7. It should be noted that the first-order solver does tend to underpredict pressure slightly, in both the steady-state and time-dependent modes. Also, the viscous–inviscid interaction of the experimental results are, of course, not captured by the Euler flow solver.

The close correlation of experimental to numerical results verify that the pressure terms for the acceleration of the control surfaces included in the boundary conditions are correct. This fact permits the investigation of airfoils that are either pitching/plunging or have no motion, and are attached to an accelerating body.

The accelerating body cases chosen were based on the test cases used previously for validation of the method. Each case was started from the steady-state solution, the body was given an acceleration, and the numerical solution was obtained over some time period. The results were then compared with the nonaccelerating case to determine the effects of the acceleration.

Because the accelerating body cases require extensive computer time, only short-duration real-time runs were performed. This was particularly true for the pitching airfoil cases, because the moving-grid algorithm was invoked for airfoil motion. Therefore, for the nonpitching airfoil cases, the real time of the run was limited to 0.1 s, whereas the entire length of the pitching airfoil run was modeled.

In addition, a concession to the computer run time was made in terms of the application of the acceleration. That is, rather than applying the acceleration in a ramped fashion, as would occur in the real world, the acceleration was applied in a sudden, or stepped, manner. Thus, the acceleration was applied instantly, which is somewhat unrealistic, but represents a limiting case.

For the nonpitching airfoil case, acceleration values of 5 and 10 g horizontal and 5 and 10 g vertical were run separately. The curves of surface pressure coefficient vs x/c at $t = 0.0050$ s are shown in Fig. 8. For this nonpitching case, the vertical accelerations produced the greatest variation in surface pressure, as anticipated.

This fact is demonstrated more visibly in Figs. 9 and 10, which are plots of C_l and C_d vs time for the nonpitching accelerated airfoil. As may be clearly seen, the vertical accelerations, after an initial jump in lift and drag caused by the step application of the acceleration, tend to reduce the value of the coefficients. On the other hand, the horizontal acceleration increases the lift and drag coefficients as time progresses.

For comparison purposes, a quasi-steady-state case was run for the 10 g vertical acceleration case, and the lift and drag coefficients were plotted in Figs. 9 and 10. It may be seen that, although the slopes of the curves are similar between the 10 g vertical case and the quasisteady case, the values of the coefficients are markedly different. Again, a portion of this effect may be attributed to the manner in which the acceleration was applied.

For the pitching airfoil, cases were run for acceleration values of 5 g horizontal and 5 g vertical simultaneously (7.07 g at 45 deg from horizontal), and 10 g horizontal and 10 g vertical simultaneously (14.14 g at 45 deg from horizontal). In

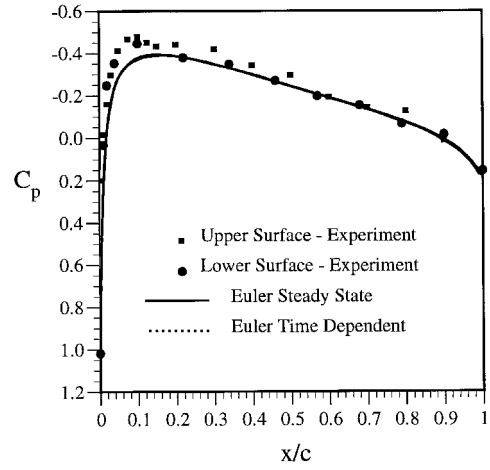

Fig. 6 Pitching airfoil at $t = 0.0$ s.

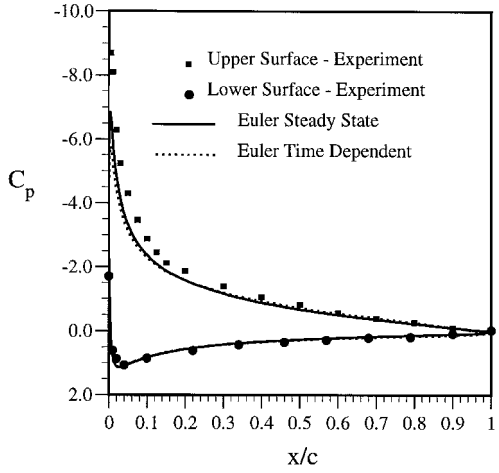

Fig. 7 Pitching airfoil at $t = 0.01642$ s.

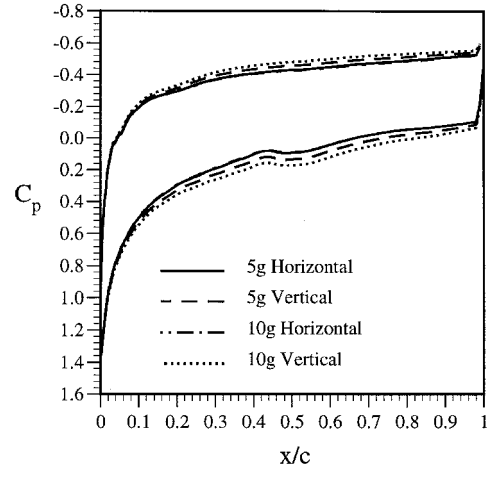

Fig. 8 Accelerated, nonpitching airfoil C_p values.

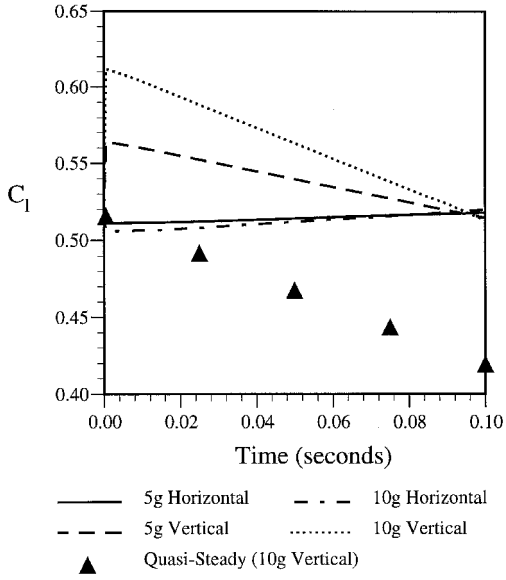

Fig. 9 Nonpitching airfoil C_l vs time.

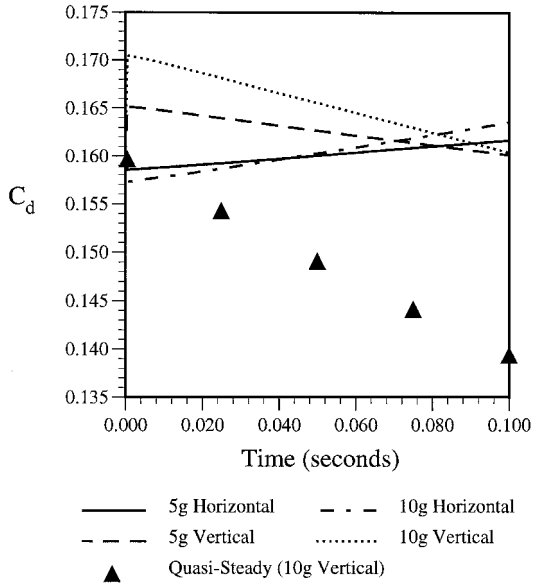

Fig. 10 Nonpitching airfoil C_d vs time.

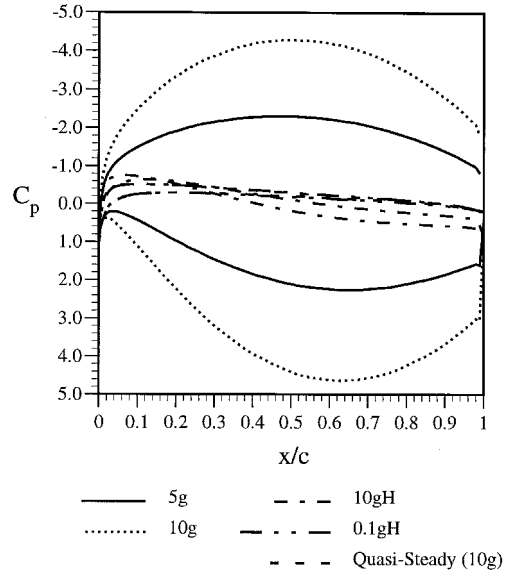

Fig. 11 Accelerating pitching airfoil C_p distribution at t = 0.00352 s.

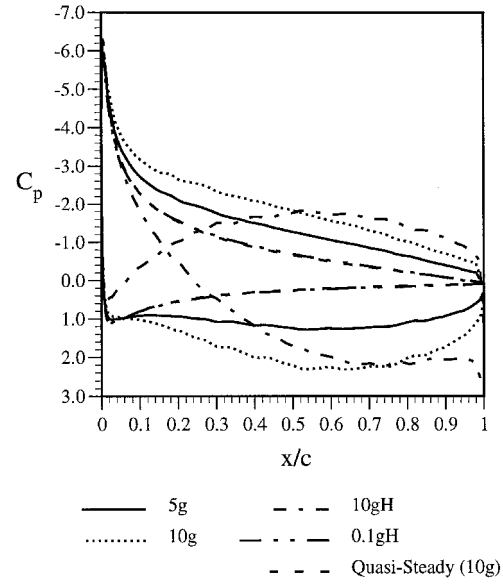

Fig. 12 Accelerating pitching airfoil C_p distribution at t = 0.01642 s.

addition, cases of 10 g horizontal, 0.1 g horizontal, and a quasi-steady-state case for the 14.14 g at 45 deg were run.

Figures 11 and 12 represent the surface pressure coefficient distribution over the pitching airfoil at t = 0.00352 s and 0.01642 s, respectively. The pitching airfoil demonstrates much greater variation in pressure because of acceleration than the nonpitching case. The initial ballooning of the pressure is partially a result of the acceleration application rate, and does tend to diminish with time, as seen in Figs. 11 and 12. However, throughout the time period of the run, substantial differences exist between the accelerated case values and the nonaccelerated case values.

Of course, this pressure variation carries over into the values of the lift and drag coefficients, as demonstrated in Figs. 13 and 14. The effect of the vertical acceleration is to decrease the lift with time, while initially increasing, and then decreasing, the drag. The horizontal acceleration has the effect of reducing the lift coefficient and drag coefficient, as compared with the nonaccelerating and quasi-steady-state cases.

To further validate the solutions obtained with this method, and to observe the effects of acceleration on the aerodynamic coefficients, the lift coefficient for the pitching airfoil case was compared to classical aerodynamic theory. The classical theory used was that of Wagner (see Ref. 22) for a thin airfoil pitching to a finite angle of attack instantly. The Wagner function is used to represent the asymptotic approach of the coefficient of lift to the steady-state value.

The lift for a section airfoil undergoing indicial pitching motion is given by Wagner as

$$L = 2\pi b \rho v w k_1(s) \tag{14}$$

where the Wagner function, $k_1(s)$, is given by Garrick[23] as

$$k_1(s) = 1 - [2/(4 + s)] \tag{15}$$

and s is the nondimensional distance traveled in terms of chord length, $s = vt/c$.

The close correlation between the lift coefficients predicted by classical theory and those of the current work is illustrated in Fig. 15. In particular, curves are shown for the pitching airfoil undergoing no linear acceleration, as well as 0.1 and 10 g horizontal accelerations.

It should be noted that both the nonaccelerating case and the 0.1 g case very closely match the classical theory. As the

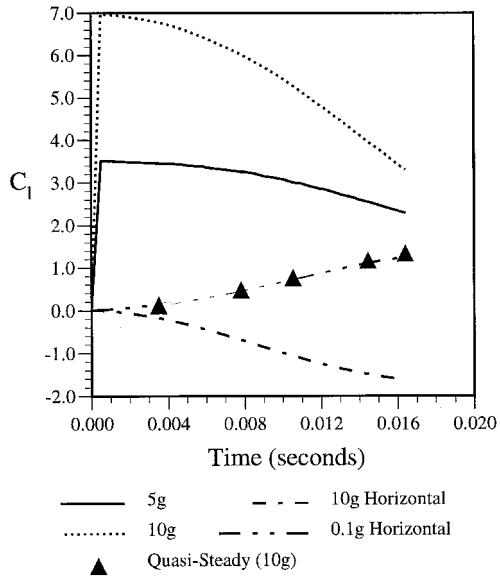

Fig. 13 Accelerating pitching airfoil C_l vs time.

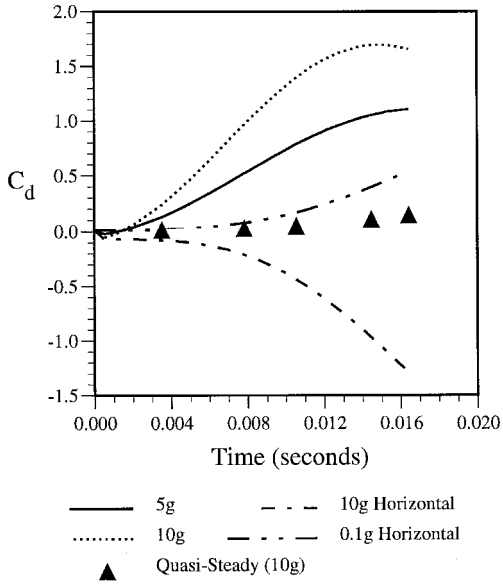

Fig. 14 Accelerating pitching airfoil C_d vs time.

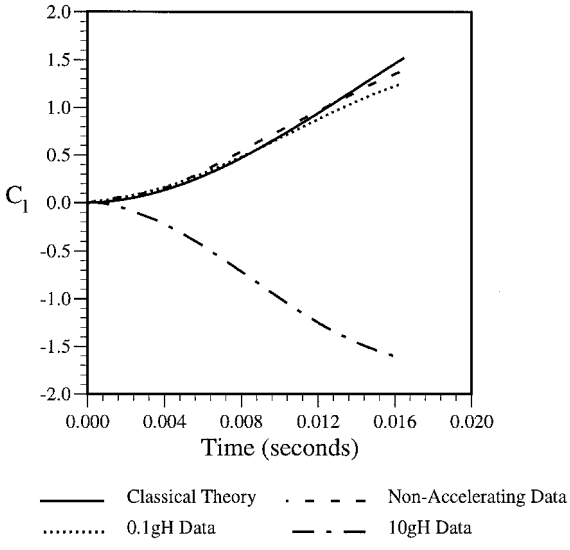

Fig. 15 C_l plot including classical theory.

horizontal acceleration is increased, the lift coefficient decreases as demonstrated by the 0.1 *g* curve, but even more dramatically by the 10 *g* curve. The nonaccelerating numerical case deviates from the classical theory by no more than 9% (below the classical value), and this occurs at the end of the pitching process. For comparison, the 0.1 *g* case, at the same point in time, predicts a lift coefficient that is 17.8% below the classical theory. The extreme case for this work, the 10 *g* horizontal acceleration case, predicts a lift coefficient that is 206.5% below the classical theory value at the end of the pitching process.

Thus, it may be clearly observed that the effect of horizontal acceleration on the lift coefficient of the pitching airfoil is to reduce the value as time progresses.

The results of this work clearly show that acceleration can contribute significantly to the values of the aerodynamics coefficients, and that it should not be neglected under certain circumstances.

Computer Requirements

All of the computations for this work were carried out on a Silicon Graphics Indigo XS at Ohio Northern University. This machine was chosen for use to evaluate the capabilities of a typically available system. The spatial grid was of unstructured format, and consisted of 2241 grid points, 6486 cell edges, and 4245 grid cells. For the steady-state solutions, the required CPU time was approximately 0.96 s/iteration. For the pitching airfoil solutions, approximately 1.6 s/iteration were required. The explicit flow solver required real time steps on the order of 3×10^{-6} s/iteration. Thus, the combination of this flow solver with a fairly slow computer means that investigations of any significant lengths of time are not practical. However, the use of a faster computational platform and explicit flow solver would make this method very useful and practical for detailed investigation of acceleration effects.

Conclusions and Recommendations

The following conclusions and recommendations are made regarding the results of this work:

1) A procedure has been developed to numerically model the effects of linear acceleration on the aerodynamics of a pitching or nonpitching airfoil. This procedure may be extended and used for aeroelastic, store separation, and adjustable engine inlet analyses, as well as a variety of others.

2) Acceleration may contribute significantly to the values of the unsteady aerodynamic coefficients, and should not be neglected under certain circumstances. In the case of this work, lift coefficients were seen to be altered by as much as 206%, based upon the type of airfoil motion and the acceleration level of the body to which the airfoil was attached.

3) The effect of horizontal acceleration is to increase the lift and drag on the nonpitching airfoil, whereas the effect upon a pitching airfoil is dependent upon the linear acceleration value and pitch rate.

4) The effect of vertical acceleration on the airfoil is as follows. The effect on the nonpitching airfoil is to decrease the lift and drag. For the pitching airfoil cases, the lift decreases, and the drag initially increases, but then subsequently decreases in value.

5) The linear acceleration should be applied in a ramped manner, as opposed to a stepped manner, to better model real-world systems.

6) The theory should be extended into three dimensions to model practical configurations. In addition, the method should be applied to general moving surface configurations, instead of simply airfoils or wings.

7) A faster flow solver and computer should be utilized to perform meaningful analyses. An implicit scheme, vectorized, and supercomputer would be appropriate.

8) The Navier–Stokes equations should be incorporated into the method to capture the viscous effects of acceleration and study vortex development and interactions.

References

[1]Huband, G. W., Rizzetta, D. P., and Shang, J. S., "Numerical Solution of the Navier-Stokes Equations for an F-16A Configuration," *Journal of Aircraft*, Vol. 26, No. 7, 1989, pp. 634–640.

[2]Shang, J. S., and Scherr, S. J., "Navier-Stokes Solution for a Complete Re-Entry Configuration," *Journal of Aircraft*, Vol. 23, No. 12, 1986, pp. 881–888.

[3]Lohner, R., and Baum, J. D., "Unstructured Grid Methods for Store Separation," *Proceedings of the 8th JOCG Aircraft/Stores Compatibility Symposium* (Fort Walton Beach, FL), 1990.

[4]Baysal, O., "Viscous Flow Simulations of Internal Store Carriage and Separation," NASA-CR-185343, July 1991.

[5]Bowman, K., Grandhi, R., and Eastep, F., "Integrated Design of Aerodynamics and Structures," AIAA Paper 89-2079, July 1989.

[6]Borland, C. J., and Rizzetta, D. P., "Nonlinear Transonic Flutter Analysis," *AIAA Journal*, Vol. 20, No. 11, 1981, pp. 1606–1615.

[7]Huttsell, L. J., and Eastep, F. E., "Aeroelastic Characteristics of NACA 0012 Airfoil at Angle of Attack," AIAA Paper 89-3375, Aug. 1989.

[8]Visbal, M. R., and Shang, J. S., "Investigation of the Flow Structure Around a Rapidly Pitching Airfoil," *AIAA Journal*, Vol. 27, No. 8, 1989, pp. 1044–1051.

[9]Shih, C., Lournenco, L. M., and Krothapalli, A., "Investigation of Flow at Leading and Trailing Edges of Pitching-Up Airfoil," *AIAA Journal*, Vol. 33, No. 8, 1995, pp. 1369–1376.

[10]Chandrasekhara, M. S., and Ahmed, S., "Velocity and Vorticity Distributions over an Oscillating Airfoil Under Compressible Dynamic Stall," *AIAA Journal*, Vol. 31, No. 6, 1993, pp. 995, 996.

[11]Ashley, S., "Thrust Vectoring: A New Angle to Air Superiority," *Mechanical Engineering*, Vol. 117, No. 1, 1995, pp. 58–64.

[12]Raymer, D. P., *Aircraft Design: A Conceptual Approach*, AIAA Education Series, AIAA, Washington, DC, 1992, pp. 336, 337.

[13]Sawyer, R. S., and Sullivan, J. P., "Lift Response of a Rectangular Wing Undergoing a Step Change in Forward Speed," *AIAA Journal*, Vol. 28, No. 7, 1990, pp. 1306, 1307.

[14]Sawyer, R. S., and Sullivan, J. P., "Unsteady Lift Development on a Constantly Accelerated Rectangular Wing," AIAA Paper 90-1633, June 1990.

[15]Ando, S., and Ichikawa, A., "Effect of Forward Acceleration on Aerodynamic Characteristics in an Inviscid Incompressible Fluid," *Transactions of the Japan Society for Aeronautical and Space Sciences*, Vol. 22, No. 56, 1979, pp. 57–69.

[16]Strang, W. Z., *Cobalt User's Manual*, WL/FIMC, Wright–Patterson AFB, OH, December 1994.

[17]Colella, P., "Glimm's Method for Gas Dynamics," *SIAM Journal on Scientific and Statistical Computing*, Vol. 3, No. 1, 1982, pp. 76–110.

[18]Batina, J. T., "Unsteady Euler Airfoil Solutions Using Unstructured Dynamic Meshes," *AIAA Journal*, Vol. 28, No. 8, 1990, pp. 1381–1388.

[19]Thomas, P. D., and Lombard, C. K., "Geometric Conservation Law and Its Application to Flow Computations on Moving Grids," *AIAA Journal*, Vol. 17, No. 10, 1979, pp. 1030–1037.

[20]"Test Cases for Inviscid Flow Field Methods," Rept. of Fluid Dynamics Panel Working Group 07, AGARD-AR-211, AGARD Advisory Rept. 211, May 1985.

[21]Landon, R. H., "NACA 0012. Oscillating and Transient Pitching," Compendium of Unsteady Aerodynamic Measurements, Data Set 3 in AGARD-R-702, Aug. 1982.

[22]Scanlan, R. H., and Rosenbaum, R., *Introduction to the Study of Aircraft Vibration and Flutter*, Dover, New York, 1968, pp. 400–405.

[23]Garrick, I. E., "On Some Reciprocal Relations in the Theory of Nonstationary Flows," NACA TR 629, 1939.